SF2A 2016
C. Reylé, J. Richard, L. Cambrésy, M. Deleuil, E. Pécontal, L. Tresse and I. Vauglin (eds)

THE CHANGING MAGNETIC FIELDS OF INTERMEDIATE-MASS T TAURI STARS

F. Villebrun[1], E. Alecian [1], J. Bouvier [1], G. Hussain [2,3] and C. P. Folsom [2]

Abstract. Through their pre-main sequence phase (PMS phase), intermediate-mass stars evolve from a fully convective structure to a radiative structure in their interiors. During this transition, the occurence of strong magnetic fields drops from 100% to 7-8%. The reasons for this drop are yet unclear, and in order to understand it we need to characterise the magnetic fields of these intermediate-mass PMS stars, and compare them with the fundamental and evolutionary properties of the stars. As a first step, we determined their effective temperatures and luminosities. We show here the ESPaDOnS and HARPSpol spectra processing that brought up our results.

Keywords: intermediate-mass stars, pre-main sequence stars, fossil magnetic fields, dynamo fields

1 Introduction

Stars at all masses appear on the HR diagram along the birthline. They start fully convective, then for more massive stars a radiative core forms and grows until the stars become fully radiative. A small convective core then develops right before they reach the Zero-Age-Main-Sequence (ZAMS). Such structural changes have important implications: during the convective phase, where the stars are either fully convective or have a convective envelope (orange and green regions in Fig. 1), magnetic fields are presumably generated via a dynamo process. In the radiative phase (the blue and pink regions in Fig. 1), no strong fields are generated in the envelope, while the dynamo field of the core takes too long to appear at the surface (e.g. Moss 2001).

The magnetic field properties of main sequence intermediate-mass stars (1.5 to $8M_{\odot}$, of spectral type A and late-B, A/B stars hereafter) are now well established. Strong magnetic fields are found in 5 to 10% of these stars. They are mainly dipolar, stable over many years and even decades (Donati & Landstreet 2009) with strengths of the order of 1 kG. Such stable and large-scale fields are called fossil fields (i.e. they are not continuously sustained from dissipation). Studies of the PMS progenitors of A/B stars, the Herbig Ae/Be (HAeBe) stars, have shown that fossil fields are present as early as the PMS phase (Alecian et al. 2013). One of the challenges today is to understand the origin of such fossil fields. The current leading theory considers that fossil fields are remnants of fields generated during the convective phase of the PMS stellar evolution. Theoretical and numerical works have demonstrated that fields generated in a previous convective phase can relax into stable fields during the transition from the convective to the radiative phase, under peculiar conditions involving the rotation rate and the proportion of poloidal to toroidal fields (Duez & Mathis 2010; Emeriau & Mathis 2015; Gaurat et al. 2015).

In addressing these issues, it is instructive to consider T Tauri stars. T Tauri stars are PMS stars of spectral types FGKM (Herbig 1962). They possess large circumstellar disks and many are still actively accreting. Intermediate-mass T Tauri stars (IMTTS, 1.2 to 4 $M_{\odot}$) are precursors to HAeBe stars. Spectropolarimetric studies of over 15 low-mass T Tauri stars have revealed that - unlike in HAeBes - magnetic fields are ubiquitous in these systems and of dynamo type (Hussain et al. 2009; Donati et al. 2008, 2010, 2011). No equivalent study has ever been performed in IMTTS. We thus want to determine the magnetic fields characteristics of IMTTS

[1] Université Grenoble Alpes, CNRS, IPAG, F-38000 Grenoble, France
[2] Institut de Recherche en Astrophysique et Planétologie, Université de Toulouse, UPS-OMP, F-31400 Toulouse, France
[3] European Southern Observatory, Karl-Schwarzschild-Str. 2, 85748 Garching bei München, Germany e-mail: ghussain@eso.org

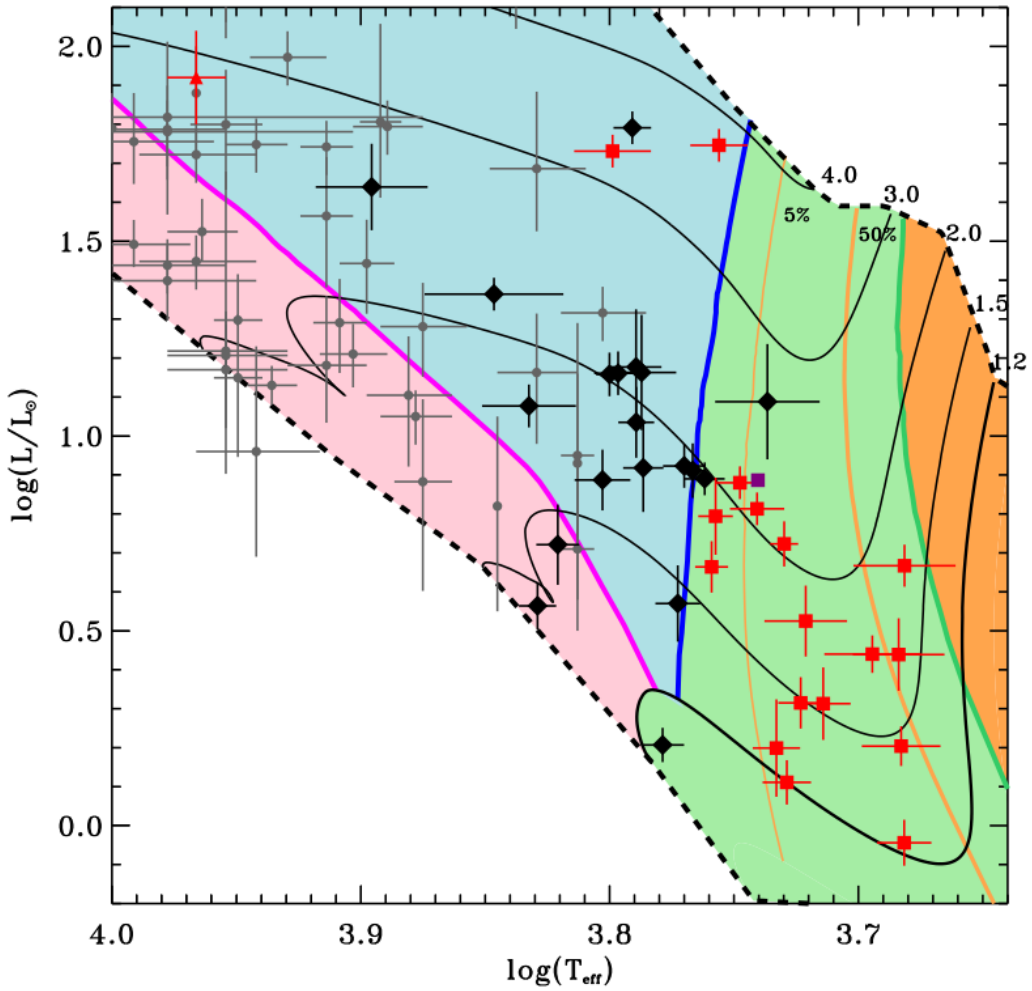

Fig. 1. IMTTS (large symbols) and some of the HAeBes (small dots) plotted in an HR diagram. Red squares are the IMTTS observed in 2012 in which a magnetic field has been detected. Black diamonds are the IMTTS observed in 2012 in which no magnetic field has been detected. The purple square (without error bars) is CV Cha, the only IMTTS with a well-constrained magnetic map (Hussain et al. 2009). The youngest magnetic HAeBe star (HD 190073) is indicated with a red triangle. The PMS evolutionary tracks (full black line) for labelled mass ($M_{\odot}$) and the ZAMS (thick dashed-line) are also overplotted. The shaded areas have the following meaning; orange: fully convective; green: radiative core + convective envelope; blue: fully radiative; and pink: convective core + radiative envelope. The thick coloured lines represent the limit between each of these regions. The 2 orange lines mark the ratio $M_{\rm conv.env.}/M_{\rm star}$ of 50% and 5%, tracing the changing internal structure of the stars. Figure updated from fig. 6 in Hussain & Alecian (2014).

(topologies, strengths and stabilities) from the fully convective region (orange) to the fully radiative region (blue). If the magnetic topology is simple, and predominantly dipolar, the field is likely fossil in origin as this is the topology found in nearly all fossil field stars. If the field is complex, multipolar, and/or has a significant toroidal component, then it is likely dynamo generated. We will thus be able to determine the time-scales and conditions in stellar interiors under which fossil fields are maintained.

Before reconstructing the surface magnetic fields of these IMTTS, we first need to determine two of their fundamental parameters : their effective temperatures $T_{\rm eff}$ and their luminosities L. $T_{\rm eff}$ and L will enable us to accurately position them in the HR diagram, providing strong constraints on their internal structure. We used the 114 ESPaDOnS and HARPSpol (respectively at CFHT and at 3.6m ESO La Silla) spectropolarimetric data of 44 IMTTS we acquired in 2012 for detecting magnetic fields in these stars. The data have been reduced using Libre-Esprit and the REDUCE software adapted for HARPSpol (e.g. Alecian et al. 2011).

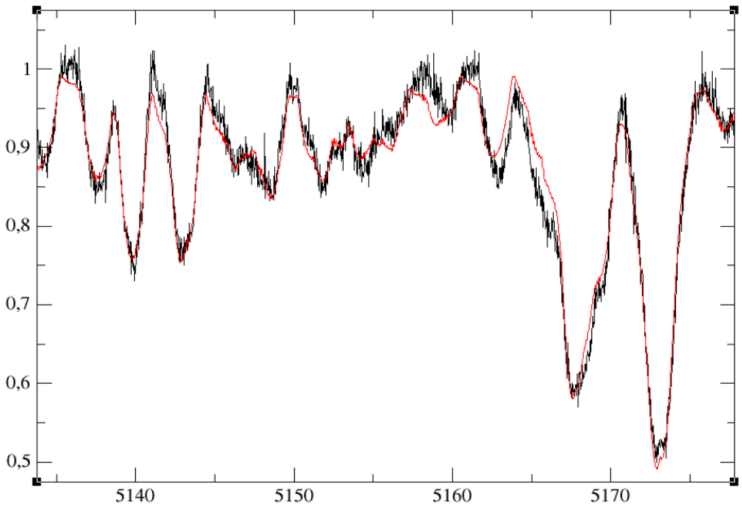

Fig. 2. Spectrum of COUP 1350 (black) measured by ESPaDOnS, and the best fit we get using the ZEEMAN spectrum synthesis code (red). Only a small portion of the spectrum is shown. As an example, for this star, we get $T_{\rm eff}$=5592.6K (σ=127.5K) and $v \sin i$=61.80km/s (σ=1.03km/s).

2 Spectra processing

2.1 Spectra renormalization

To derive the stars' effective temperatures, the spectrum synthesis code ZEEMAN (Landstreet 1988; Wade et al. 2001; Folsom et al. 2012) needs accurately normalized spectra. The normalization provided by the data reduction pipeline being insufficient for our work, we used a polynomial renormalization routine (C. Folsom, PhD Thesis, Sect 5.1). This routine determines continuum points in the stellar spectrum order by order, and then fits a polynomial function based on these continuum points. The original spectrum is then divided by the fitted polynomial function, making sure that the spectrum is sufficiently well-normalized for our study. For high-$v \sin i$ stars, renormalization can be challenging as line broadening can make the continuum difficult to determine. We therefore need to be much more cautious when continuum-fitting the spectra of rapidly rotating stars ($v \sin i > 80$km/s) by selecting continuum points with more demanding standards.

2.2 Spectra fitting

Once properly normalized, we used the spectrum synthesis code ZEEMAN and stellar atmospheric models from MARCS (Gustafsson et al. 2008) to derive stellar parameters. By a χ^2-minimization procedure (see Fig. 2) ZEEMAN makes every non-fixed stellar parameter converge to its best solution. To get a better accuracy on the parameters we were interested in ($T_{\rm eff}$ and $v \sin i$) we reduced the number of degrees of freedom by setting all the other stellar parameters to the reference quantities used for these stars: log(g)=4.0, $v_{\rm macro}$ = 2km/s, and solar abundances (Asplund et al. 2009). We discarded wavelength windows that fall into one of the following cases: potentially affected by telluric lines, potentially affected by emission lines, bad quality fits (with a high RMS difference with respect to the rest of the spectrum), close to the blue-edge (noise is high here), close to the red-edge (many telluric lines at high λ). By using as much spectral information as possible for each spectrum, 2-6 spectra for each IMTTS of our sample, and by excluding bad quality fits with a 1 or 2 σ-clipping, we derived $T_{\rm eff}$ and $v \sin i$ with typical uncertainties of $\sim$ 120K and $\sim$ 1.5km/s respectively (450K and 20km/s for the most challenging cases, respectively).

2.3 Luminosity determination

To position our sample of IMTTS in the HR diagram, we also needed to compute their luminosities. We based our calculations on the (V-J) band, (B-V) being more affected by accretion and circumstellar extinction. We took the J magnitudes from the 2MASS survey (Cutri et al. 2003) and the V magnitudes mainly from Kharchenko (2001), or from the NOMAD catalog (Zacharias et al. 2004). We used theoretical $(\text{V-J})_o$ of 5-30 Myr intermediate-mass stars from Pecaut & Mamajek (2013) to compute the color excesses E(V-J) and extinctions A_J. The total to selective extinction R_J=0.437 has been determined from the color excesses and extinctions relationships shown in Casagrande et al. (2010). We then used new GAIA parallaxes (Gaia Collaboration et al. 2016) to determine the absolute magnitudes M_J of our stars, and theoretical bolometric corrections $(BC)_J$ from

Pecaut & Mamajek (2013) to get their bolometric magnitudes. Finally, using $M_{bol\odot}$=4.74 from Cox (2000), we determined their bolometric luminosities. For a dozen of stars, GAIA parallaxes were not available: we thus used the best distance estimate of their corresponding star-forming region/cluster found in the literature.

3 Conclusion

Our estimates of $T_{\rm eff}$ and luminosities are displayed on the HR diagram with their associated error bars (see Fig 1.). Preliminary studies of our spectropolarimetric data indicate that about half of our IMTTS are magnetic (red) contrary to the non-magnetic ones (black). We find that almost all stars in the convective regions (orange and green) are magnetic. Once the envelope of the stars becomes fully radiative (blue and pink regions) the magnetic incidence drops dramatically, implying that a drastic selection must be made.

To determine the circumstances of this selection, we plan to map the surface magnetic fields of IMTTS in the convective region (green). Mapping the surface magnetic fields of IMTTS at different stages of their evolution through the PMS will enable us to compare these magnetic fields with the fundamental and evolutionary properties of these stars, which are now better constrained thanks to the determination of $T_{\rm eff}$ and L that we performed.

This work has made use of data from the European Space Agency (ESA) mission *Gaia* (`http://www.cosmos.esa.int/gaia`), processed by the *Gaia* Data Processing and Analysis Consortium (DPAC, `http://www.cosmos.esa.int/web/gaia/dpac/consortium`). Funding for the DPAC has been provided by national institutions, in particular the institutions participating in the *Gaia* Multilateral Agreement.

Villebrun F. is financed by the AGIR program of the Université Grenoble Alpes.

References

Alecian, E., Kochukhov, O., Neiner, C., et al. 2011, A&A, 536, L6

Alecian, E., Wade, G. A., Catala, C., et al. 2013, MNRAS, 429, 1001

Asplund, M., Grevesse, N., Sauval, A. J., & Scott, P. 2009, ARA&A, 47, 481

Casagrande, L., Ramírez, I., Meléndez, J., Bessell, M., & Asplund, M. 2010, A&A, 512, A54

Cox, A. N. 2000, Allen's astrophysical quantities

Cutri, R. M., Skrutskie, M. F., van Dyk, S., et al. 2003, VizieR Online Data Catalog, 2246

Donati, J.-F., Bouvier, J., Walter, F. M., et al. 2011, MNRAS, 412, 2454

Donati, J.-F., Jardine, M. M., Gregory, S. G., et al. 2008, MNRAS, 386, 1234

Donati, J.-F. & Landstreet, J. D. 2009, ARA&A, 47, 333

Donati, J.-F., Skelly, M. B., Bouvier, J., et al. 2010, MNRAS, 402, 1426

Duez, V. & Mathis, S. 2010, A&A, 517, A58

Emeriau, C. & Mathis, S. 2015, in IAU Symposium, Vol. 307, New Windows on Massive Stars, ed. G. Meynet, C. Georgy, J. Groh, & P. Stee, 373–374

Folsom, C. P., Bagnulo, S., Wade, G. A., et al. 2012, MNRAS, 422, 2072

Gaia Collaboration, Brown, A. G. A., Vallenari, A., et al. 2016, ArXiv e-prints

Gaurat, M., Jouve, L., Lignières, F., & Gastine, T. 2015, A&A, 580, A103

Gustafsson, B., Edvardsson, B., Eriksson, K., et al. 2008, A&A, 486, 951

Herbig, G. H. 1962, Advances in Astronomy and Astrophysics, 1, 47

Hussain, G. A. J. & Alecian, E. 2014, in IAU Symposium, Vol. 302, Magnetic Fields throughout Stellar Evolution, ed. P. Petit, M. Jardine, & H. C. Spruit, 25–37

Hussain, G. A. J., Collier Cameron, A., Jardine, M. M., et al. 2009, MNRAS, 398, 189

Kharchenko, N. V. 2001, Kinematika i Fizika Nebesnykh Tel, 17, 409

Landstreet, J. D. 1988, ApJ, 326, 967

Moss, D. 2001, in Astronomical Society of the Pacific Conference Series, Vol. 248, Magnetic Fields Across the Hertzsprung-Russell Diagram, ed. G. Mathys, S. K. Solanki, & D. T. Wickramasinghe, 305

Pecaut, M. J. & Mamajek, E. E. 2013, ApJS, 208, 9

Wade, G. A., Bagnulo, S., Kochukhov, O., et al. 2001, A&A, 374, 265

Zacharias, N., Monet, D. G., Levine, S. E., et al. 2004, in Bulletin of the American Astronomical Society, Vol. 36, American Astronomical Society Meeting Abstracts, 1418